Surfaces and Interfaces 4 (2016) 69–76

Contents lists available at ScienceDirect

Surfaces and Interfaces

journal homepage: www.elsevier.com/locate/surfin

Nanoscale investigations: Surface potential of rare-earth oxide (Re_2O_3) thin films by kelvin probe force microscopy for next generation CMOS technology

Pawan Kumar, Robin Khosla, Satinder K. Sharma*

School of Computing and Electrical Engineering, Indian Institute of Technology (IIT)-Mandi, MANDI, Himachal Pradesh-175001, India

ARTICLE INFO

Article history:
Received 1 June 2016
Revised 29 July 2016
Accepted 22 August 2016
Available online 17 September 2016

Keywords:
High-κ
Thin films
Er_2O_3
CPD
KPFM
Rapid thermal annealing
Furnace annealing

ABSTRACT

Here, the surface morphology, quantitative surface charge injection in nanoscale regime, spreading, decay and physical significance of trap charges are systematically investigated on furnace annealed (FA) and rapid thermal annealed (RTA) ultrathin rare earth oxide (Re_2O_3), Er_2O_3/Si structure by Kelvin probe force microscopy (KPFM). The computed charge decay and contact potential difference (CPD) are found as a strong function of injected charges along with the type of subjected post deposition annealing treatment. The RTA treated Er_2O_3 films showed higher CPD value (~266 mV) and lowest charge spreading (~2.1 μm) for trapped holes than the FA (CPD ~196 mV and charge spreading ~2.27 μm). The CPD for negative bias are computed higher (~196 mV and ~266 mV) than that of the corresponding positive (~−184 mV and ~-229 mV) in both FA and RTA treated Er_2O_3/Si structures, respectively. It reveals easier holes trapping than electrons and n-type nature of sputtered Er_2O_3 ultrathin films. There is a significant ~80% vertical charge decay and ~20% lateral spreading for first 60 min due to conjunction of effective injected and polarization charges. Thus, the FA and RTA treated Er_2O_3 films are potential candidates for CMOS and NVRAM applications, respectively.

1. Introduction

The scaling of device feature size for integrated circuits (IC's), secure charge retention for data storage in ultrathin dielectric films is a key issue for nonvolatile semiconductor memories (NVSM) due to stringent demands of superior performance, low-power operation, high reliability and low cost [1,2]. With the scaling of dielectric films thickness at nanometer regime, the dielectric surfaces and interfaces play a dominant role, whereas the exact mechanism for charge storage and decay at nanoscale regime is not clear till date. Thus, the meticulous charge trapping/de-trapping and surface potential analysis of the dielectric layer are the major challenges in front of device and process engineers for next technology node [3–5]. Although, as the thickness of traditional gate dielectric SiO_2, approached to the nano-metric regime high static power dissipation became a hurdle for extending the scaling to next level of technology node. Thus, to sustain scaling trends at lower power dissipation, the next generation IC industry attracted towards the high-κ based quality oxides not only for complementary metal-oxide-semiconductor (CMOS) technology but also for NVSM device applications i.e. NAND, NOR FLASH, FeRAM, MRAM, PCRAM and ReRAM [6–8]. Even though, majority of high-κ oxides are not stable at high temperature due to the formation of polycrystalline phase and finally ends up with the degradation of memory devices reliability, due to dominant leakage paths caused by grain boundaries in polycrystalline phase. Additionally, the epitaxial growth of single crystal high quality, high-κ oxides are difficult to account of process technology and also not cost effective. Therefore, exploitation of amorphous high-κ oxide as a possible future alternate prospective with superior thermal stability, excellent electrical and physical properties is still an open challenge. In this respect, numerous high-κ dielectric such as: HfO_2 [8–9], ZrO_2 [10], Al_2O_3 [11], and rare earth oxides (Er_2O_3, Y_2O_3, La_2O_3, Pr_2O_3) are investigated in the past decade for metal-oxide-semiconductor (MOS) and non-volatile semiconductor memory (NVSM) device applications [12–14]. From high-κ oxides, Er_2O_3 arose as a promising contender as alternate gate dielectric, due to high dielectric constant (~12-20), thermodynamic and kinetic stability, higher conduction band offset, good interface and lower leakage current density [7,15–17]. Over and above especially with higher Gibbs free energy of ~122 Kcal/mol, provides excellent thermodynamic stability at elevated temperatures [18]. Therefore, the systematic investigation of charge trapping/de-trapping and surface characteristics of Er_2O_3 (high-κ) ultrathin films, prior to its integration with

* Corresponding author. Fax: +91 01905-267075.
E-mail address: satinder@iitmandi.ac.in (S.K. Sharma).

http://dx.doi.org/10.1016/j.surfin.2016.08.003
2468-0230/

real world IC's technology is of enormous importance. In this consequence, systematic investigations of post deposition annealed (PDA) Er_2O_3, especially nano scale surface morphological analysis and surface potential decay in the form of trap charges with lateral spreading over few micrometer scales is imperative for next generation memory device applications. Although, there are various well established techniques found in literature for surface potential analysis of dielectric systems such as photoelectron spectroscopy (PES), and scanning electron microscopy (SEM) with electron beam induced current analysis, Kelvin probe (KP) and Kelvin probe force microscopy (KPFM) [19] etc. Granting all this, KPFM is a nondestructive, cutting-edge and reliable technique with higher spatial resolution which provides highly localized electrical properties at nanoscale. Over and above, KPFM provides direct visualization of trapped charge and charge decay quantitatively in terms of, contact potential difference (CPD) variation of the injected charge with time onto dielectric surface. Moreover, in IC's processing, conventional furnace annealing (FA) and rapid thermal annealing (RTA) are extensively used techniques for PDA treatments to modify the oxide/dielectric layers interface [20–22]. In literature, it is well reported from the investigations of Miritello et al. (2006) and Deqiet al. (2009) etc. [23–31], that PDA treatment plays a vital role to improve the quality of dielectric films in terms of performance and reliability. However, surface morphology, quantitative surface charge spreading properties and decay mechanism (e.g.: lateral and vertical decay), physical significance behind the trap charges (e.g.: surface, injected and polarization charges) and the nature of Er_2O_3 is needed to be methodologically investigated. In this work, Er_2O_3 ultrathin films are deposited by RF-magnetron sputtering and subjected to PDA treatment with FA and RTA. The post deposition FA and RTA treated Er_2O_3/Si interface was analysed by cross-sectional High Resolution Transmission Electron Microscopy (HRTEM). The trapping and de-trapping dynamics of charges in Er_2O_3 ultrathin films have been studied by KPFM technique. The surface morphology, quantitative surface charge spreading properties and decay mechanism, physical significance behind the trap charges are systematically investigated. It was observed that higher CPD value in RTA, Er_2O_3 ultrathin films are feasible as a trapping layer in charge trapping non-volatile semiconductor memories (NVSM). Conversely, the lower CPD value in FA, Er_2O_3 films reveals its feasibility as an alternate gate dielectric for CMOS technology.

2. Experimental

The ⟨100⟩ orientation p-type silicon wafers with resistivity of 1–10 Ω cm were used in this study. After standard Radio Corporation of America (RCA) cleanings, the native oxide was removed in diluted (1%) hydrofluoric acid (HF) solution and thoroughly rinsed in deionized (DI) water. After drying these RCA cleaned silicon wafers in N_2, wafers were used for Er_2O_3 ultrathin (~8.21 nm measured by Accurion EP3 imaging ellipsometer) films deposition by Techport RF-magnetron sputtering system. The distance of erbium target from wafers surface was kept constant ~7 cm. At the outset, the ultimate pressure of sputtering system was $\sim 5 \times 10^{-6}$ torr and then deposition of ultrathin Er_2O_3 films was carried out at R.F power 60 W, pressure of Ar/O_2 (45:5 sccm) and temperature of 27 °C on the RCA cleaned silicon wafers. One set of the above ultrathin Er_2O_3 films deposited Si wafers were subjected to rapid thermal annealing at 700 °C for 30 sec at ramp rate of 30 °C/sec in N_2 and second set of ultrathin Er_2O_3 films deposited Si wafers were subjected to furnace annealing at 700 °C for 30 min in inert atmosphere of N_2. The charge injection and contact potential differences (CPD) analysis experiments were performed at ambient condition with AFM (Dimension Icon from Bruker). The conducting MESP Co/Cr coated AFM probes (from Bruker) with frequency, 60–100 kHz and spring constant, 1–5 N/m were used for the charge injection and KPFM study. Initially, the charge injection on ultrathin Er_2O_3 films surfaces was performed under standard AFM contact mode. For charge injection, −3 and + 3 V bias was applied to the tip for electrons and holes injection respectively, on Er_2O_3/Si system for optimum time (injected charge saturation) of 10 min and the substrate kept at ground potential. During charge injection, the Er_2O_3 ultrathin films get polarized, when the bias is removed the trapped charges remains in the Er_2O_3 ultrathin films as shown in schematic of Fig. 1(d)–(f). Afterwards, for CPDs analysis, the images of injected charges were visualized under non-contact (lift) mode with optimized lift height (minimizes the interference between the tip and the sample) of ~100 nm, as shown in Fig. 1(f). CPDs data acquisition was performed in interleaved line by line scan mode with sample topography analysis and tip was kept at ground potential. KPFM measurement of the sample surfaces were acquired with the cantilever vibrating at a slightly lower frequency (~2 KHz) than its resonance frequency and at a probe scan rate of 0.99 Hz. Furthermore, the KPFM feedback parameters were adjusted to an optimized magnitude for minimization of error profile. The protruding range of error profile with best contrast fit for KPFM imaging was found well below ± 5 mV. In this analysis, contact potential difference magnitude variations with the time domain was computed by KPFM at a periodicity of 8 min. Albeit, all the KPFM micrographs based surface potential analysis accomplished in the form of contact potential difference (CPD) for post deposition treated furnace and rapid thermal annealed, Er_2O_3/Si systems were performed through the standard centre line profile scheme. The crystallinity of Er_2O_3 ultrathin films was characterized by Grazing Incidence X-ray Diffraction (GIXRD) (given in Supplementary Information - Fig. S1) using Rigaku Smartlab System at 0.5° angle. The interface of Er_2O_3/Si system was analyzed by HRTEM of FEI, USA.

3. Results and discussions

Fig. 2 shows the cross-sectional HRTEM images of Er_2O_3/Si interface for Furnace [Fig. 2(a)] and Rapid thermal [Fig. 2(b)] post deposition annealing treated Er_2O_3 ultrathin films. It is clearly observed that rapid thermal post deposition annealing treatment result the formation of small interfacial layer (SiO_2/Er-Si-O) at the Er_2O_3/Si interface whereas furnace based post deposition annealing treatment result the sharp Er_2O_3/Si interface. This unintentional interfacial layer is probably due to structural re-orientation and relaxation that takes place simultaneously at Er_2O_3/Si interface due to high ramp up rate in rapid thermal processing and results the defects at interface through the breaking of old bonds and formation of newer one of the Er–O and Si–O onto Er_2O_3/Si interface. Therefore, post deposition FA treated Er_2O_3 thin films are superior as compared to RTA treated Er_2O_3 thin films as gate dielectric for CMOS technology because the low dielectric constant interfacial layer (SiO_2/Er-Si-O) formation during post deposition RTA treatment decrease the overall dielectric constant of gate stacks and hence diminishes the scaling advantages which are achieved using high-κ.

The surface topography of the post deposition furnace and rapid thermal annealed Er_2O_3 ultrathin films at 700 °C for 30 min and 30 sec, respectively, are analyzed with a standard tapping mode atomic force microscopy (AFM) technique. The surface roughness (r.m.s), measured for $5 \times 5\ \mu m^2$ scan area of FA [Fig. 3(a), (b)] and RTA [Fig. 3(c), (d)], ultrathin Er_2O_3 films are ~0.45 and ~0.60 nm, respectively. The higher surface roughness of Er_2O_3 ultrathin films treated with RTA than FA might be due to high ramp up rate in rapid thermal processing which results the residual compressive stresses. Likewise, interfacial layer formation also conformed at the Er_2O_3/Si interface from HRTEM micrograph [Fig. 2(b)]. Hence,

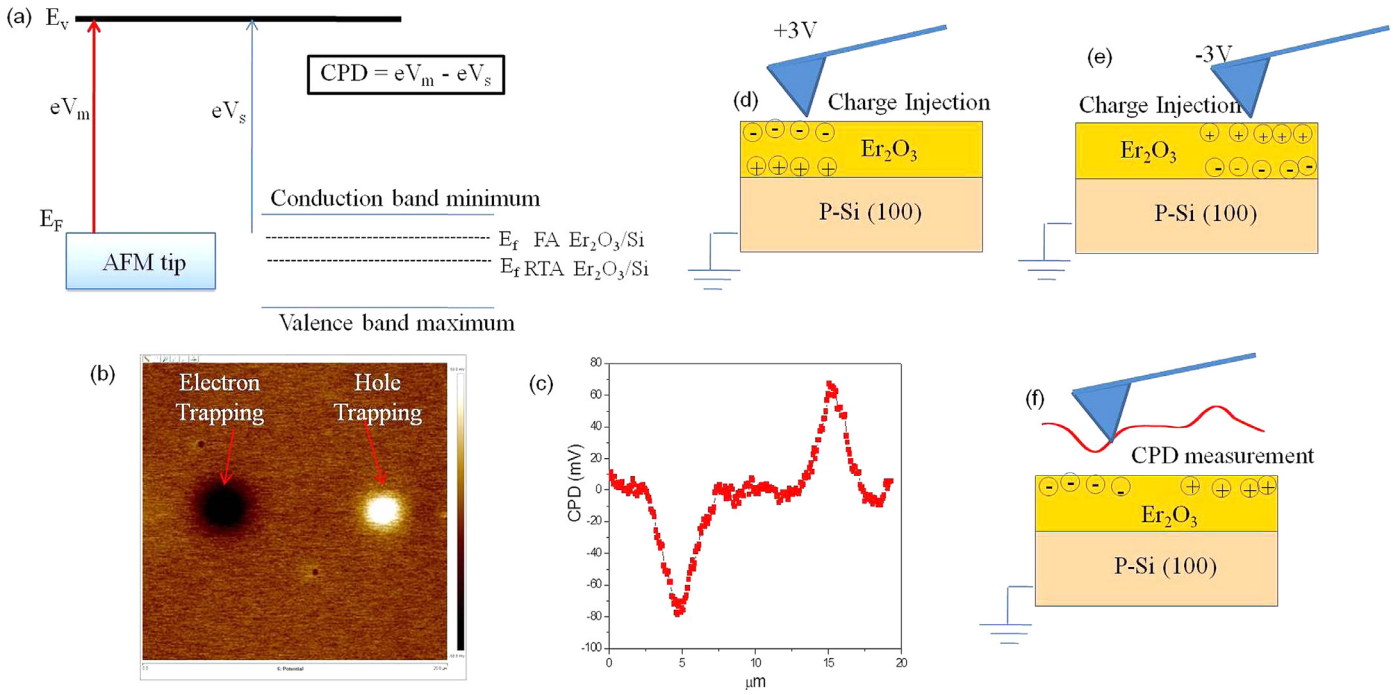

Fig. 1. Schematic for (a) Flat band structure, showing the location of the Fermi level for furnace and rapid thermal post deposition annealed Er_2O_3 ultrathin films, (b) Surface potential KPFM images immediately after electrons and holes injection, (c) CPD measurements obtained by drawing horizontal line across the injection center. Er_2O_3/Si structure and KPFM analysis method, (d) & (e) charge injection in contact mode and (f) Contact Potential Difference (CPD) measurement in non-contact (lift) mode with lift height of 100 nm.

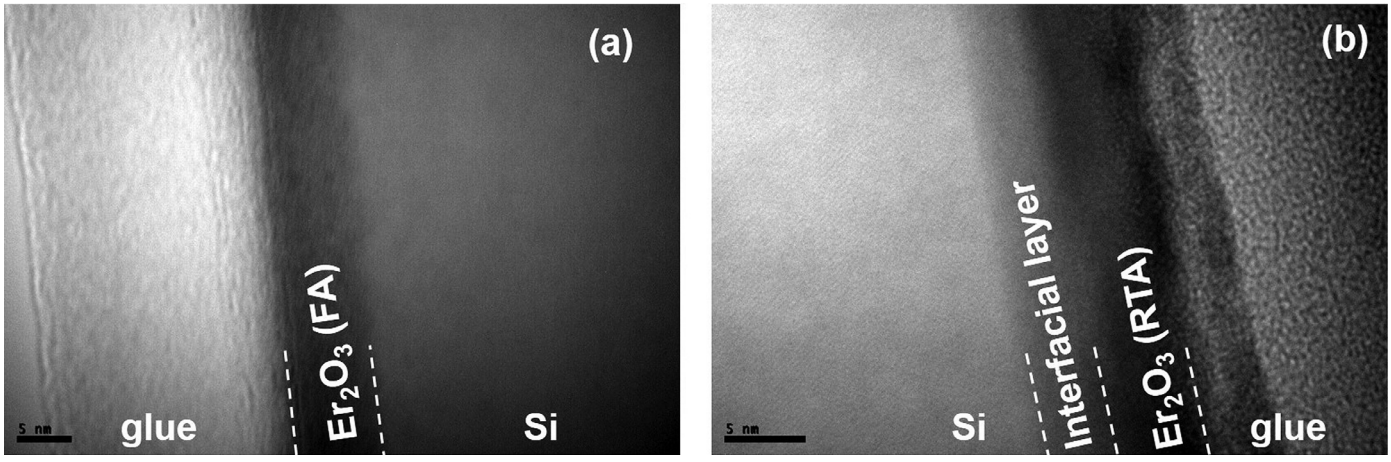

Fig. 2. HRTEM cross-section images of Er_2O_3/Si interface after (a) Furnace and (b) Rapid thermal annealing treatment.

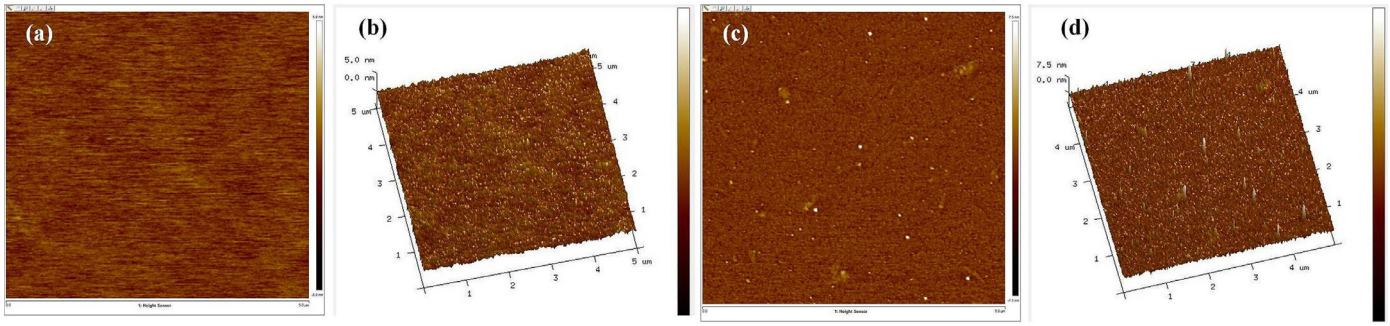

Fig. 3. (a) 2D, (b) 3D AFM micrograph of furnace annealed, and (c) 2D, (d) 3D AFM micrograph of rapid thermal annealed Er_2O_3 ultrathin films on Si substrate.

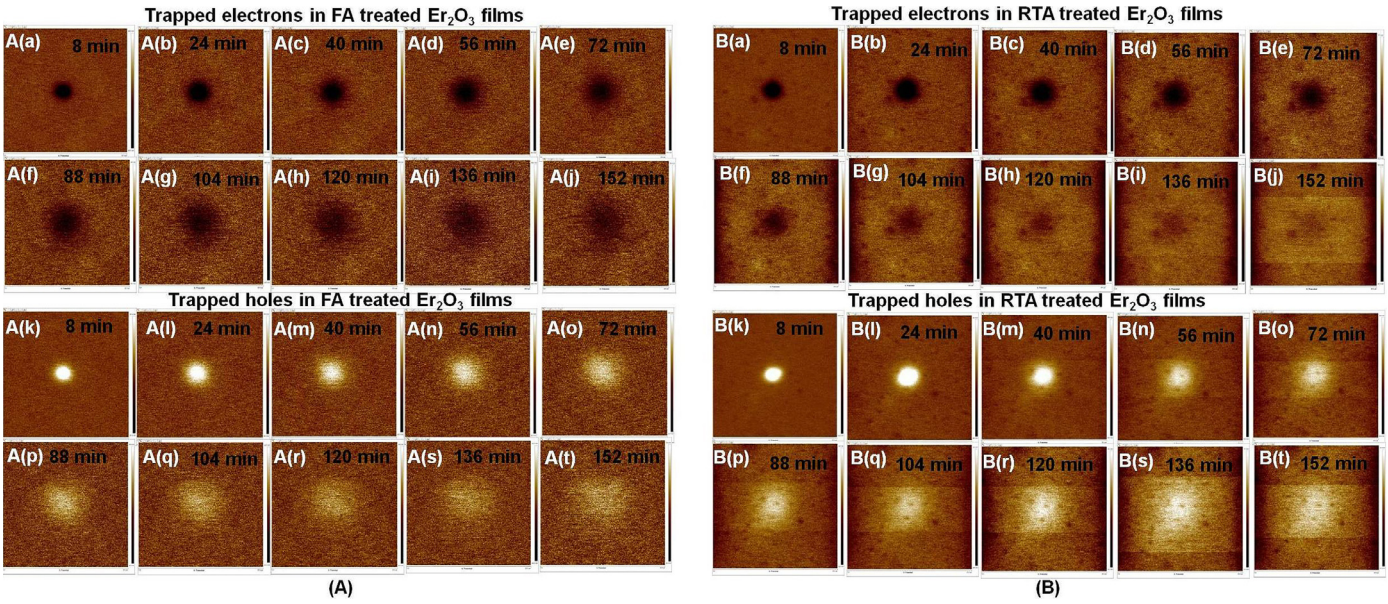

Fig. 4. The KPFM surface potential (CPD) images of FA treated Er_2O_3 ultrathin film for trapped electrons A(a)-A(j), trapped holes A(k)-A(t) and for RTA treated Er_2O_3 ultrathin film for trapped electrons B(a)-B(j), trapped holes B(k)-B(t) measured after decay time of 8 min, 24 min, 40 min, 56 min, 72 min, 88 min, 104 min, 120 min, 136 min, and 152 min respectively.

the post deposition RTA treated Er_2O_3/Si structure consists slightly higher surface roughness ~0.15 nm.

Fig. 4 shows the KPFM surface potential micrographs (CPD images) after the charge injections through the conducting AFM cantilever tip, which results the trapping of electrons and holes in post deposition FA treated Er_2O_3 ultrathin films. Though, for subsequent charge injection, an optimal (for maximum injection after set of experiments) charge injection bias +3 V and −3 V were applied at two different regions of interest (ROI) on surface of FA based PDA treated Er_2O_3/Si structure, for holes and electrons injection, respectively. Certainly, the charge injection in Er_2O_3/Si system is concomitant with the work function difference between AFM cantilever tip and Er_2O_3 ultrathin films surface of Er_2O_3/Si system. It results the shifting of fermi energy levels, and is verified from the CPD values [Fig. 1(a) and (c)]. Though, the KPFM is an outstanding, established technique, appropriate for ultrathin films (< 50 nm) surface potential investigations. Because, it divulges the information about spatially surface charge distribution of ultrathin films, owing to the existence of discrete atomic levels, electrostatic interactions between a conductive AFM cantilever tip and sample surface. Therefore, the CPD values of Er_2O_3/Si system was computed in this work using KPFM technique by following relation:

$$CPD = \frac{\Phi_{tip} - \Phi_{sample}}{e} \quad (1)$$

Here, Φ_{tip} (eV_m), Φ_{sample} (eV_s) and e, is the surface potential of conducting AFM cantilever tip, the surface potential of Er_2O_3 ultrathin film surface and fundamental electronic charge, respectively. Thus, as depicted from KPFM, Fig. 4 micrographs, the existence of white and black province at ROI, corresponds to holes and electrons trapping, respectively after charge injection on FA based PDA treated Er_2O_3/Si system. Thereafter, a successive, CPD scans were performed, after every 8 minutes incremental intervals on the charge injected Er_2O_3 film surfaces. Fig. 4A(a) to (j) and Fig. 4A(k) to (t) micrographs show the injected electrons and holes trapped, respectively in FA treated Er_2O_3/Si system and correspondingly, CPD profile contrast variations measured on time domain from 8 to 152 min. Even though, it is well established that the presence of a sharp contrast by virtue of a higher charge injection or trapped charged density in KPFM micrographs of ultrathin films, undoubtedly apparent from higher magnitude of the CPD value. As examined from Fig. 4A(a) to (j), the dullness in injected charge spot contrast from 8 to 152 min for black ROI (trapped electrons) is more as compared to white ROI (trapped holes) of Fig. 4A(k) to (t). It evidently reveals higher charge decay and spreading of trapped electrons in contrast to holes in FA based PDA treated Er_2O_3/Si structure [32]. Similarly, Fig. 4B(a) to (j) and Fig. 4B(k) to (t) represents KPFM surface potential micrographs (CPD images) for trapped electrons (black ROI) and holes (white ROI) after charge injection of RTA based PDA treated Er_2O_3/Si system. The CPD scanning measurements were followed with analogous method as stated earlier, for FA based PDA treated system. As noticed from Fig. 4B(a) to (j) for black region (trapped electrons) the dullness in injected charge spot contrast is more than white regions (trapped holes) for Fig. 4B(k) to (t). It unquestionably indicates higher charge decay and spreading of trapped electrons as compared to holes for RTA based PDA treated Er_2O_3/Si system [32].

As depicted from Fig. 5(b) & (d), the CPD values of trapped holes are ~196 and ~266 mV for FA and RTA based PDA treated Er_2O_3 ultrathin films of Er_2O_3/Si systems. This noticeably higher CPD magnitude of RTA, Er_2O_3/Si system signifies manifestation of the higher number of holes trapping density as compared to conventional FA based PDA treated Er_2O_3/Si systems. Correspondingly, the CPD values for trapped electrons [Fig. 5(a) & (c)] are ~−184 mV for FA and ~−229 mV for RTA based PDA treated Er_2O_3 ultrathin films. It is once again anticipated that the higher CPD magnitude for RTA than FA based PDA treated Er_2O_3 conspicuous to the higher electrons trapping. It attributes that during RTA treatment structural re-orientation and relaxation takes place simultaneously at Er_2O_3/Si interface and originates effective oxide charges and defects through the breaking of old bonds and formation of newer one of the Er–O and Si–O onto Er_2O_3/Si interface [36,37]. So, this increase of trap density in RTA based Er_2O_3 ultrathin films is due to increase in effective oxide traps which result in the higher charge trapping in Er_2O_3/Si system after RTA treatment. The extensive details of various computed CPD values, at numerous charge decay scale by KPFM, for Er_2O_3 ultrathin films of Er_2O_3/Si structures are given in supplementary information (Table S1). As

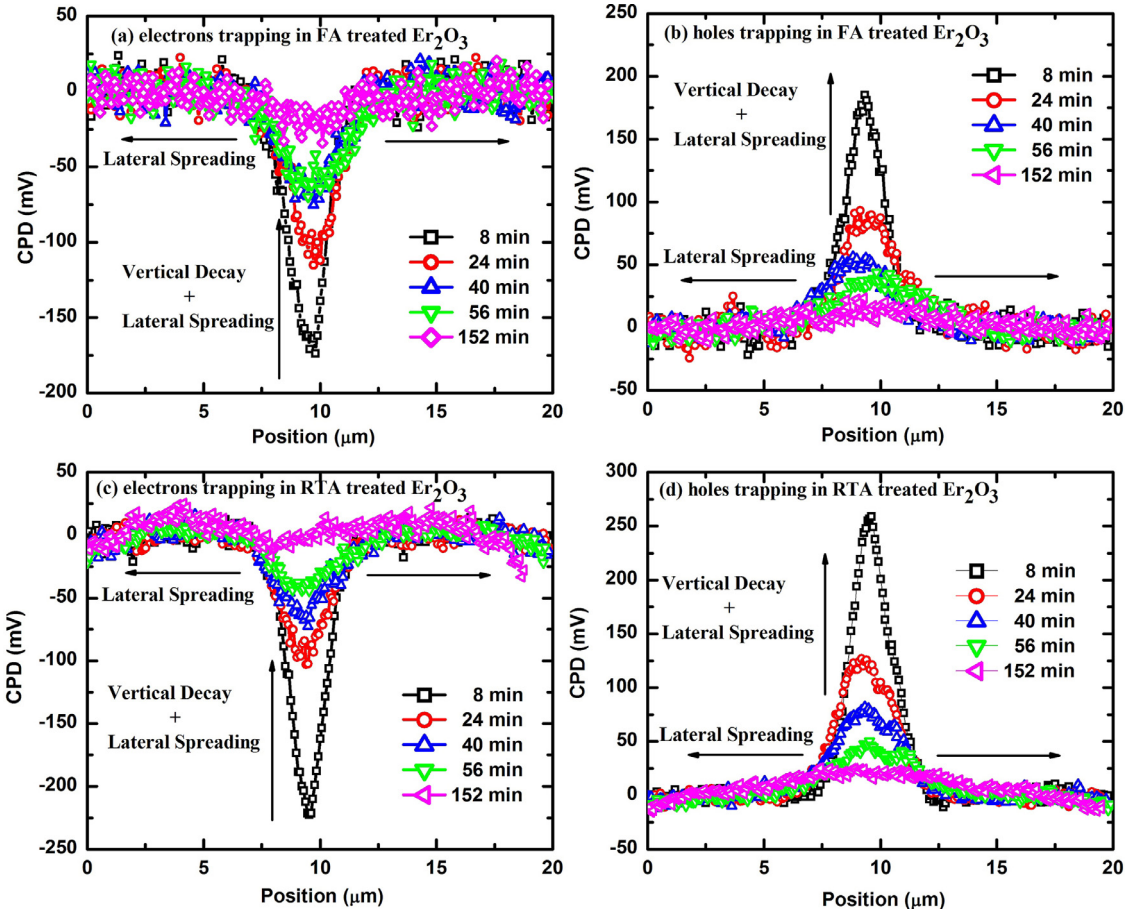

Fig. 5. CPD line profile for (a) electrons trapping, (b) holes trapping in FA based PDA treated Er_2O_3/Si and CPD line profile for (c) electrons trapping, (d) holes trapping in RTA based PDA treated Er_2O_3/Si system.

perceived from Table S1, there is clearly noticeable disparity in CPD magnitude for negative bias charge injection of both cases. Here, it is quite interesting to note that CPD values for negative charge injection biases (holes trapping) were higher than the positive charge injection biases (electron trapping) at same voltage (say 3 V). It demonstrates the higher probability of holes trapping than electron trapping in Er_2O_3 ultrathin films. Next to this, the higher CPD value for holes trapping in contrast to electrons for both FA and RTA based PDA treated Er_2O_3 ultrathin films of Er_2O_3/Si system at room temperature reveals the n-type nature of Er_2O_3 ultrathin films [33]. This may be explained due to two reasons: (i) higher electron mobility (μ_e) than hole mobility (μ_h) in Er_2O_3, can result in higher CPD value for hole, less hole spreading and hence small charge decay as compare to electron; (ii) possibility of dominant donor interface traps at the Er_2O_3/Si interface, which are positive when empty and neutral when full [28].

Even though it is well established that the CPD computed through the standard KPFM technique at an optimized bias has a contribution of three main fundamental factors (i) surface charges/screen charges (ii) injected charges and (iii) polarization charges induced by the applied bias between conducting AFM probe and sample [32]. Whereas, the effect of surface charges in the computed CPD can be get rid of by the grounding of tip during KPFM scan as accomplished here [34]. Thus, the computation of CPD in the present work, is a result of two contributions, i.e. firstly injection and secondary polarization charges. Therefore, to measure and establish the contribution of surface charges, the CPD scans were executed with and without grounded tip for both furnace and rapid thermal based PDA treated Er_2O_3 ultrathin films of Er_2O_3/Si systems as shown in Fig. 6. As identified from Fig. 6(a) to (d), that during grounded tip scan, the CPD value decay, especially for negatively biased ROI (~38 mV shown in Fig. 6(a)) is lower than the positive biased ROI (~−50 mV shown in Fig. 6(b)) in RTA based PDA treated Er_2O_3/Si systems. On the contrary for FA based PDA treated Er_2O_3/Si systems, the CPD value decay for negative biased ROI (~50 mV shown in Fig. 6(c)) is higher than the positive biased ROI (~−45 mV shown in Fig. 6(d)). It inevitably demonstrates that under negative bias, majority of stored charges are injected and polarization, whereas under positive bias, surface charges also have modest contributions to measured CPD values, chiefly in case of RTA treated Er_2O_3/Si systems [34]. Aside from the CPD values contingent upon the FA treated Er_2O_3 ultrathin films exhibited that charges decay for grounded tip scan is mostly same magnitude for both negative and positive bias (~50 mV and ~−45 mV), indicates less disparity in CPD decay for positive and negative bias. Hence it demonstrates that the majority of trapped charges are injected and polarization charges in both positively and negatively biased regions of Er_2O_3 ultrathin films of Er_2O_3/Si systems. Henceforth, there is trivial contribution of surface charges towards effective computed CPD magnitude of Er_2O_3/Si systems in the course of KPFM scans of present work [34]. Though, the polarization charges together with injected charges contributes to the CPD value, due to rotation of dielectric dipoles under the influence of applied electric field (i.e. between AFM tip and Er_2O_3 dielectric surface) in Er_2O_3 ultrathin films. Thus, it concludes that effective residual CPD magnitude is due to injection and polarization charges only. While, the charge decay in both FA and RTA based PDA treated Er_2O_3 ultrathin films of Er_2O_3/Si systems take place in principally two

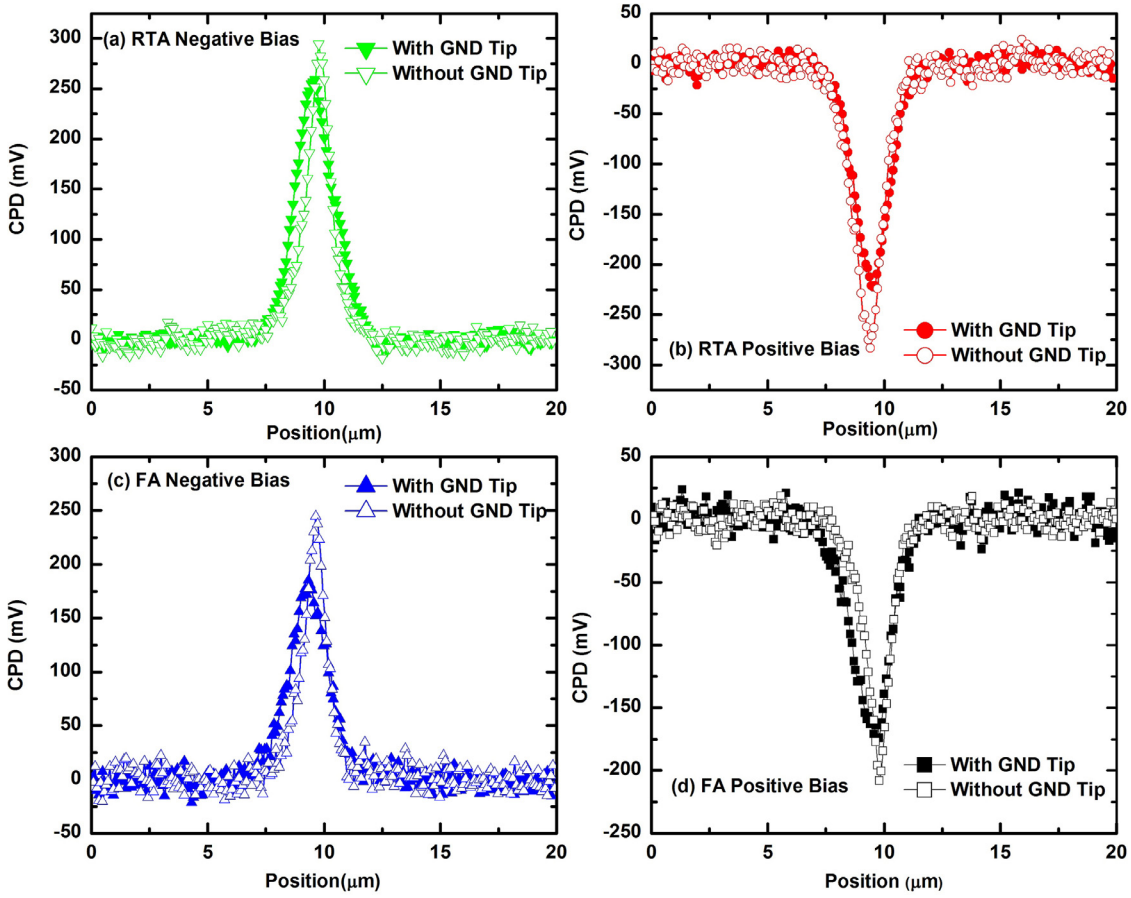

Fig. 6. The contact potential difference (CPD) value plot with and without grounded tip scan for (a) negative bias, (b) positive bias for RTA treated Er_2O_3/Si systems and (c) negative bias, (d) positive bias for FA treated Er_2O_3/Si systems.

fundamental charge transport mechanisms vertical and lateral [35]. Initially, the charges were injected along 200 nm, *x*-axis (ROI) direction and disabled *y*-axis (ROI) directional scan. Thereafter, KPFM scan was followed after 8 minute and noticed that the initially injected charge (200 nm) ROI spread along the region of ~ 2 μm, as shown in Fig. 4A(a) to (j) and Fig. 4B(a) to (j). These distributions of injected charges were also proven from the variation of CPD magnitude as presented in Fig. 5(a) to (d). It attributes that initially during the charge injection, there was lateral charge spreading on the Er_2O_3 film surface (during charge injection i.e. before KPFM measurement) prominent mechanism for charge distribution, while after 8 min aging vertical decay was dominant mechanism for charge transportation as revealed in Fig. 5(a) to (d). Thus, it demonstrates that vertical decay plays a dominant role in degradation of retention characteristics of MOS based systems. As noticed with the aging of charge loss, charge is observed to decay due to both vertical decay and lateral spreading as shown in Fig. 5(a) to (d). Fig. 5 shows that majority of charges are lost through vertical decay, while lateral spreading is suppressed dramatically (as indicated by arrow in Fig. 5(a) & (b)). Therefore, to decouple the contribution of vertical and lateral charge decay from the computed CPD profile an approximation method is used here [34]. The charge density decay is calculated by a trapezoid method, which consists of lateral spreading distance (Δ_s) and vertical charge loss (ρ_m), given by the following relation [36]:

$$\Delta_s(\tau) = \frac{w_0}{2}\frac{\varphi(|w_0|,\tau)}{\varphi(0,\tau)-\varphi(|w_0|,\tau)} \quad (2)$$

$$\rho_m(\tau) = \frac{2\varepsilon}{{w_0}^2}(\varphi(0,\tau)-\varphi(|w_0|,\tau) \quad (3)$$

Fig. 7(a) & (b), shows the calculated value of ρ_m and Δ_s, normalized for better perspective of charge decay mechanisms. A decrease in ρ_m of ~80% is observed in first 60 min and increase in Δ_s of ~20%, which evidently reveals that vertical (electrons and holes) charge decay was fundamental mechanism for this duration [34]. Furthermore, for first 60 min ρ_m is higher (8%) for trapped electrons as compared to holes (4%) in RTA treated Er_2O_3 ultrathin films, as revealed form plot of Fig. 7(a). Likewise, Fig. 7(b) clearly shows that in RTA Er_2O_3 ultrathin films, Δ_s for holes is lowest which is comparable with the measured spreading distance as shown in supplementary information (Table S2). Fig. 7(c) shows that the injected charge spreading ~2.9 and ~3.0 μm for electrons and ~2.1 and ~2.2 μm for holes of RTA and FA based PDA treated Er_2O_3 ultrathin films of Er_2O_3/Si systems, respectively. Furthermore, in the beginning particularly for FA based PDA treated Er_2O_3/Si systems holes spreading (~2.27 μm) is less than the electron charge spreading (~3.06 μm) but after 56 min the holes spreading (~5.13 μm) become large as compared to electrons spreading (~4.63 μm). On the other hand, for RTA based PDA treated Er_2O_3 ultrathin films of Er_2O_3/Si systems the electrons spreading are significantly higher than holes spreading even after 152 min. Fig. 7(d) shows the variation of computed CPD values measured from KPFM analysis as a function of time domain. As indicated that injected electrons and holes decay, measured after consecutive 8 min interval. It is visibly observed that the CPD values for both electrons and holes are higher and decreases exponentially for RTA process as compared to FA. Along with, it is also perceived that the charge transferred to the Er_2O_3 ultrathin films surfaces disappear readily within the first 60 min. Whereas, after this interval the reduction trend in CPD value profile seems almost parallel and constant. This indicates that a nearly similar electrons

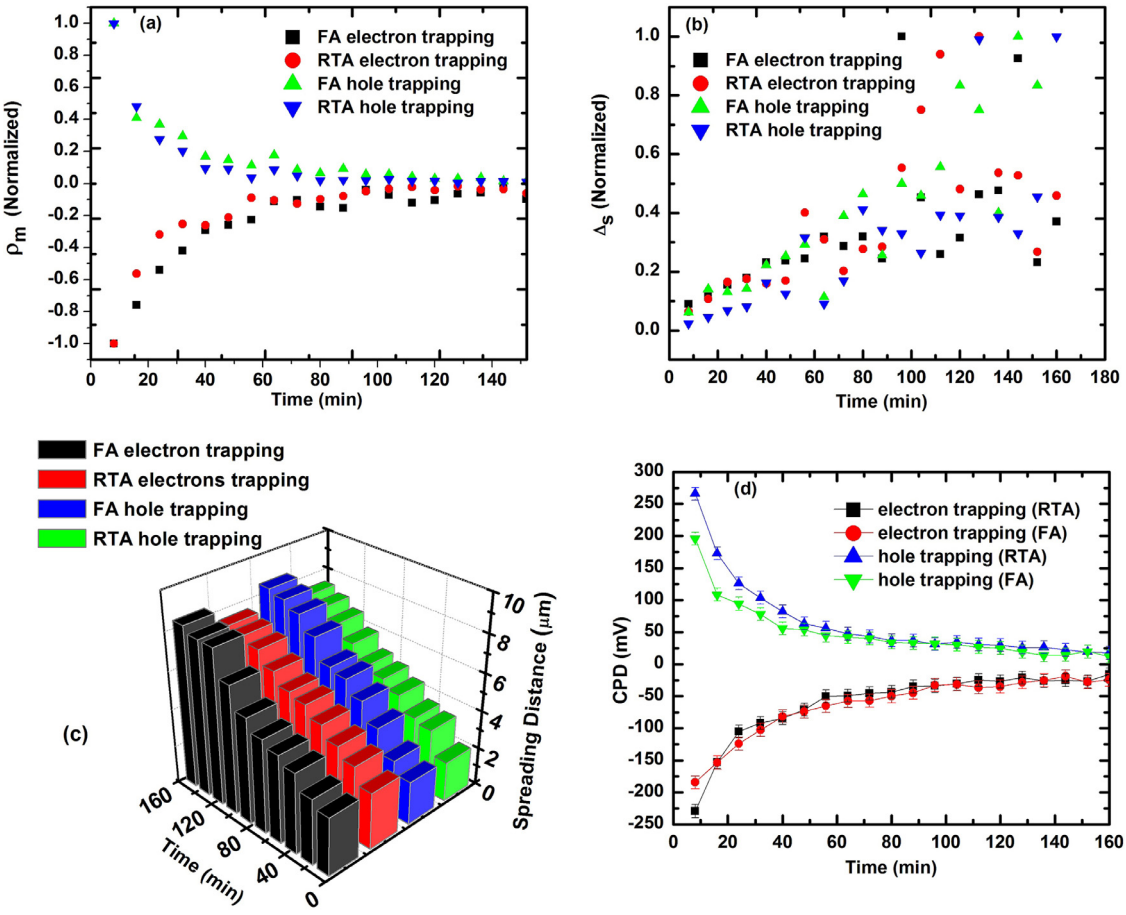

Fig. 7. Charge decay analysis with aging. (a) Normalized maximum charge density (ρ_m), (b) Normalized Lateral charge distance (Δ_s), (c) Total lateral charge spreading distance (Δ_t), and (d) CPD variations, of the trapped electrons and holes with respect to decay time for FA and RTA based PDA treated Er_2O_3 ultrathin films.

and holes density trapped in the Er_2O_3 ultrathin films of Er_2O_3/Si structures for both cases.

Moreover, as shown in supplementary information (Table S2), the lateral spreading distance (2.1 μm) is smaller in RTA as compared to FA treated Er_2O_3/Si system. This signifies the higher charge trapping proficiency of the rapid thermal process than conventional furnace based PDA treated Er_2O_3 ultrathin films of Er_2O_3/Si system. Typically, the effective positive oxide traps generation occurs at the high-κ/semiconductor structure due to interfacial restructuring via reorientation of atoms [36]. Here, it is apparent that during RTA treatment structural re-orientation and relaxation takes place simultaneously at Er_2O_3/Si interface and originate effective oxide charges and defects at the interface through the breaking of old bonds and formation of newer one of the Er–O and Si–O onto Er_2O_3/Si interface [36–38]. So, this increase of trap density in RTA based Er_2O_3 ultrathin films may be due to increase in effective oxide traps in Er_2O_3/Si interface after RTA treatment. These observations reveal that due to presence of higher number of traps, the charge trapping will be higher in RTA based PDA treated Er_2O_3 ultrathin films of Er_2O_3/Si structure. Therefore, RTA treated Er_2O_3 ultrathin film is a potential candidate as charge trapping material for non-volatile memory device applications; while FA treated Er_2O_3 ultrathin films are more reliable for CMOS device applications.

4. Conclusion

We have investigated the charge decay and lateral charge spreading properties of trapped charges for RTA and FA based PDA treated Er_2O_3 ultrathin films of Er_2O_3/Si structures by KPFM. The higher CPD values for holes in both FA and RTA based PDA treated Er_2O_3 ultrathin films of Er_2O_3/Si systems, signify the more probability of holes trapping as compared to electrons and imply the n-type nature of Er_2O_3 ultrathin films under ambient conditions. The charge decay mechanism of the Er_2O_3 ultrathin films is studied and vertical decay is found to be dominant mechanism in contrast to lateral charge spreading especially for RTA treated Er_2O_3 ultrathin films. The cross-sectional HRTEM analysis of Er_2O_3/Si interface reveals that post deposition RTA treatment results in formation of small interfacial layer (SiO_2/Er-Si-O) at the Er_2O_3/Si interface whereas FA treatment results in sharp Er_2O_3/Si interface. Furthermore, the higher charge trapping capability of RTA based PDA treated Er_2O_3 ultrathin films of Er_2O_3/Si structures were observed, due to the presence of more number of interfacial traps, polarization charges in high-κ/Si system than FA treated Er_2O_3/Si structures. Thus, the FA and RTA based PDA treated Er_2O_3 ultrathin films are potential candidates for CMOS device applications and non-volatile scaled memory device applications, respectively with enhanced performance and reliability.

Acknowledgements

We acknowledge Indian Nanoelectronics Users Program (INUP) and the facility technologists for the use of sample preparation facility at Centre for Nano Science and Engineering (CeNSE), Indian Institute of Science (IISc), Bangalore, India. Author S.K.S also acknowledges the financial support of seed grant project

IIT/SG/SKS/27, Indian Institute of Technology (IIT), Mandi, (H.P), India

Supplementary materials

Supplementary material associated with this article can be found, in the online version, at doi:10.1016/j.surfin.2016.08.003.

References

[1] C. Zhao, C.Z. Zhao, S. Taylor, P.R. Chalker, Review on non-volatile memory with high-k dielectrics: flash for generation beyond 32 nm, Materials 7 (2014) 5117–5145.

[2] International Technology Roadmap for Semiconductors (ITRS). http://public.itrs.net/Links/2013ITRS/Summary2013.html, 2013.

[3] E. Lusky, Y. Shacham-Diamand, A. Shappir, I. Bloom, B. Eitan, Traps spectroscopy of the Si3Ni4 layer using localized charge-trapping nonvolatile memory device, Appl. Phys. Lett. 85 (2004) 669.

[4] T.H. Kim, J.S. Sim, J.D. Lee, H.C. Shin, B.-G. Park, Charge decay characteristics of silicon-oxide-nitride-oxide-silicon structure at elevated temperatures and extraction of the nitride trap density distribution, Appl. Phys. Lett. 85 (2004) 660.

[5] K.B. Jinesh, Y. Lamy, E. Tois, W.F.A. Besling, Charge conduction mechanisms of atomic-layer-deposited Er_2O_3 thin films, Appl. Phys. Lett. 94 (2009) 252906.

[6] M.H. Kryder, C.S. Kim, After hard drives—what comes next? IEEE Trans. Magn. 45 (2009) 3406.

[7] R. Khosla, D.K. Sharma, S.K. Sharma, Effect of electrical stress on $Au/Pb(Zr_{0.52}Ti_{0.48})O_3/TiO_xN_y/Si$ gate stack for reliability analysis of ferroelectric field effect transistors, Appl. Phys. Lett. 105 (2014) 152907.

[8] D.K. Sharma, R. Khosla, S.K. Sharma, Multilevel metal/Pb $(Zr_{0.52}Ti_{0.48})O_3/TiO_xN_y/Si$ for next generation FeRAM technology node, Solid-State Electron. 111 (2015) 42–46.

[9] P. Ren, R. Wang, X. Jiang, Y. Qiu, C. Liu, R. Huang, Experimental study on the oxide trap coupling effect in metal oxide semiconductor field effect transistors with HfO_2 gate dielectrics, Appl. Phys. Lett. 104 (2014) 263512.

[10] J.S. Lee, S. Chang, S.M. Koo, S.Y. Lee, High-performance a-IGZO TFT with ZrO_2 gate dielectric fabricated at room temperature, IEEE Electron Device Lett. 31 (2010) 225–227.

[11] B. Lee, G. Mordi, M.J. Kim, Y.J. Chabal, E.M. Vogel, R.M. Wallace, K.J. Cho, L. Colombo, J. Kim, Characteristics of high-k Al_2O_3 dielectric using ozone-based atomic layer deposition for dual-gated graphene devices, Appl. Phys. Lett. 97 (2010) 043107.

[12] H. Yabuta, M. Sano, K. Abe, T. Aiba, T. Den, H. Kumomi, K. Nomura, T. Kamiya, H. Hosono, High-mobility thin-film transistor with amorphous InGaZnO4 channel fabricated by room temperature rf-magnetron sputtering, Appl. Phys. Lett. 89 (2006) 112123.

[13] F.H. Chen, J.L. Her, Y.H. Shao, Y.H. Matsuda, T.M. Pan, Structural and electrical characteristics of high-κ Er_2O_3 and Er_2TiO_5 gate dielectrics for a-IGZO thin–film transistors, Nanoscale Res. Lett. 8 (2013) 18.

[14] T.M. Pan, T.Y. Yu, Comparison of the structural properties and electrical characteristics of Pr_2O_3, Nd_2O_3 and Er_2O_3 charge trapping layer memories, Semicond. Sci. Technol. 24 (2009) 095022.

[15] H.S. Kamineni, V.K. Kamineni, R.L. Moore, S. Gallis, A.C. Diebold, M. Huang, A.E. Kaloyeros, Optical and structural characterization of thermal oxidation effects of erbium thin films deposited by electron beam on silicon, J. Appl. Phys. 111 (2012) 013104.

[16] J. Robertson, High dielectric constant oxides, Eur. Phys. J. Appl. Phys. 28 (2004) 265.

[17] A.R. Chaudhuri, A. Fissel, H.J. Osten, Superior dielectric properties for template assisted grown (100) oriented Gd_2O_3 thin films on Si (100), Appl. Phys. Lett. 104 (2014) 012906.

[18] K.J. Hubbarda, D.G. Schlom, Thermodynamic stability of binary oxides in contact with silicon, J. Mater. Res. 11 (1996) 2757.

[19] W. Melitz, J. Shen, A.C. Kummel, S. Lee, Kelvin probe force microscopy and its application, Surf. Sci. Rep. 66 (2011) 1–27.

[20] S. Spiga, F. Driussi, A. Lamperti, G. Congedo, O. Salicio, Effects of thermal treatments on the trapping properties of HfO_2 films for charge trap memories, Appl. Phys. Exp. 5 (2012) 021102.

[21] K. Zhu, Y. Yang, J. Huang, Y. Lu, J. Li, R. Tan, P. Cui, W. Song, Effects of rapid thermal annealing on electrical transport in heavily doped ZnO thin films deposited at different substrate temperatures, J. Electron. Mater. 43 (2014) 3973–3978.

[22] K.Y. Cheong, W. Bahng, N.-K. Kim, Effects of rapid thermal annealing on nitrided gate oxide grown on 4H-SiC, Microelectron. Eng. 83 (2006) 65–71.

[23] C.H. Kao, H. Chen, Y.T. Pan, J.S. Chiu, T.C. Lu, The characteristics of the high-K Er_2O_3 (erbium oxide) dielectrics deposited on polycrystalline silicon, Solid State Comm. 152 (2012) 504–508.

[24] K.B. Jinesh, Y. Lamy, E. Tois, W.F.A. Besling, Charge conduction mechanisms of atomic-layer-deposited Er_2O_3 thin films, Appl. Phys. Lett. 94 (2009) 252906.

[25] M. Miritello, R. Lo Savio, A.M. Piro, G. Franzò, F. Priolo, Optical and structural properties of Er_2O_3 films grown by magnetron sputtering, J. Appl. Phys. 100 (2006) 013502.

[26] W. Deqi, Y. Jincheng, Z. Hongsheng, C. Aimin, L. Feng, Leakage current mechanisms of ultrathin high-k Er_2O_3 gate dielectric film, J. Semicond. 30 (2009) 103003.

[27] R. Xu, C.G. Takoudis, Atomic layer deposition and characterization of amorphous$Er_xTi_{1-x}O_y$dielectric ultra-thin films, ECS J. Solid State Sci. Tech. 1 (2012) N107–N114.

[28] E.H. Nicollian, J.R. Brews, MOS (Metal Oxide Semiconductor) Physics and Technology, Wiley Classics Library ed., John Wiley & Sons, New Jersey, 2003.

[29] Z.B. Fang, S. Chen, Y.Y. Zhu, Y.Q. Wu, Y.L. Fan, Y.Y. Wang, Z.M. Jiang, Structural and electrical characterization of ultrathin Er_2O_3 films grown on Si(001) by reactive evaporation, Nanotechnology 18 (2007) 155205.

[30] F. Ze-Bo, Z.Y. Yan, W. Jia-Le, J.Z. Min, Annealing effects on the structure and electrical characteristics of amorphous Er_2O_3 films, Chin. Phys. B 18 (2009) 3542.

[31] R. Khosla, P. Kumar, S.K. Sharma, Charge trapping and decay mechanism in post deposition annealed Er_2O_3 MOS capacitors by nanoscopic and macroscopic characterization, IEEE Trans. Device Mater. Rel. 15 (2015) 610–616.

[32] J. Xu, J. Xu, Y. Wang, Y. Cao, W. Li, L. Yu, K. Chen, Microscopic and macroscopic characterization of the charging effects in SiC/Si nanocrystal/SiCs and witched structures, Nanotechnology 25 (2014) 055703.

[33] G. Hao, Z. Huang, Y. Liu, X. Qi, L. Ren, X. Peng, L. Yang, X. Wei, J. Zhong, Electrostatic properties of few-layer MoS_2 films, AIP Adv. 3 (2013) 042125.

[34] A. Kumar, T.S. Herng, K.Y. Zeng, J. Ding, Bipolar charge storage characteristics in copper and cobalt co-doped Zinc Oxide (ZnO) thin film, ACS Appl. Mater. Interf. 4 (2012) 5276–5280.

[35] K.Y. Cheong, W. Bahng, N.-K. Kim, Effects of rapid thermal annealing on nitrided gate oxide grown on 4H-SiC, Microelectron. Eng. 83 (2006) 65–71.

[36] S.J. Baik, K.S. Lim, W. Choi, H. Yoo, J.-S. Lee, H. Shin, Lateral redistribution of trapped charges in nitride/oxide/Si (NOS) investigated by electrostatic force microscopy, Nanoscale 3 (2011) 2560–2565.

[37] Y. Han, Z. Huo, X. Li, G. Chen, X. Yang, D. Zhang, Y. Wang, Investigation of charge loss mechanism of thickness-scalable trapping layer by variable temperature Kelvin probe force microscopy, IEEE Electron Device Lett. 34 (2013) 870–872.

[38] T. Huang, K.M. Wong, M. Li, X. Zhu, K.M. Lau, Effect of post-gate RTA on leakage current (Ioff) in GaN MOSHEMTs, Phys. Status Solidi C 9 (2012) 919–922.